ResearchGate

See discussions, stats, and author profiles for this publication at: https://www.researchgate.net/publication/376459575

Thermal and Signal Integrity Improvement in a 3D RRAM Crossbar with Carbon Nanotube Interconnects

Conference Paper · October 2023

DOI: 10.1109/NMDC57951.2023.10343766

CITATION
1

READS
31

5 authors, including:

Khitem Lahbacha
Università degli studi di Cassino e del Lazio Meridionale
15 PUBLICATIONS **60** CITATIONS
SEE PROFILE

Fakhreddine Zayer
Khalifa University
34 PUBLICATIONS **160** CITATIONS
SEE PROFILE

Belgacem Hamdi
University of Sousse
93 PUBLICATIONS **592** CITATIONS
SEE PROFILE

Wael Dghais
Institute of Telecommunications
64 PUBLICATIONS **426** CITATIONS
SEE PROFILE

All content following this page was uploaded by Khitem Lahbacha on 05 April 2024.

The user has requested enhancement of the downloaded file.

2023 IEEE Nanotechnology Materials and Devices Conference (NMDC) | 979-8-3503-3546-0/23/$31.00 ©2023 IEEE | DOI: 10.1109/NMDC57951.2023.10343766

Thermal and Signal Integrity Improvement in a 3D RRAM Crossbar with Carbon Nanotube Interconnects

Khitem Lahbacha, *Member*, *IEEE,* Fakhreddine Zayer, Hamdi Belgacem, Wael Dghais, *Member, IEEE*, and Antonio Maffucci, Senior Member, IEEE

***Abstract*— The focus of this paper is to explore the implementation of resistive random-access memory (RRAM) cells in monolithic integration while addressing the reliability issues that can affect the efficiency of the memory. Specifically, the paper addresses the use of Nickel (Ni) interconnects as a conventional material and the high resistivity and temperatures resulting from Set/Reset switching. The paper proposes using carbon nanotubes (CNT) as an alternative material to improve signal and thermal integrity. The paper analyzes the electrothermal 1D1R structure and compares the conventional Ni metal electrodes to the CNT ones using a full 3D numerical model to provide electrical and thermal responses. The study enhances the accuracy of the model by considering the temperature-dependent electrical and thermal conductivity of the conductive filament and oxide. The paper also introduces a new structure called 1D1R-1R1D that allows for resistive switching for all layers and increases the density of the crossbar memory while addressing problems with the conventional structure. The paper analyzes the issues of voltage drop along wires and thermal crosstalk in both horizontal and vertical directions. The results of this study demonstrate the potential benefits of CNT interconnects for improving the thermal and signal integrity of RRAM crossbars.**

***Keywords*— 3D RRAM crossbar; Carbon nanotubes; electro-thermal effects; 1D1R-1R1D; Signal integrity; Thermal integrity.**

II. Introduction

The development of new information technologies has rapidly progressed according to Moore's law, resulting in an increased demand for higher data storage density. Traditional methods of improving storage density through miniaturization are limited, and new structures and mechanisms are needed for reliable performance [1]-[3]. Emerging memories offer promising solutions for next-generation storage, with 3D materials offering superior thermal and electrical properties. Resistive Random Access Memory (RRAM) is a promising alternative due to its scalability, fast read/write speed, and low power consumption. The simple RRAM structure and its small feature size make it particularly suitable for high-density integration [4],[5]. RRAM devices are made of various materials, including hafnium oxide (HfOx) and titanium oxide, which allow for switching phenomena. HfOx-based RRAM has excellent resistive behavior, and resistive switching occurs through the formation and breakage of the conductive filament under externally applied voltage. However, thermal effects can cause unwanted filament breakage due to Joule heating [6]. Therefore, the choice of electrode materials is crucial for memory performance. Several rigid contact electrodes metal materials have been so far used for RRAM such as Ag, Al, Pt, Cu, Ti, and Ni [7],[8].

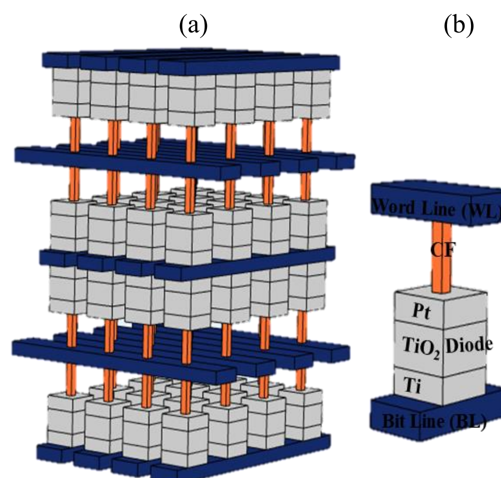

Figure 1. 4×4×4 3D 1D1R-1R1D crossbar RRAM structure. b) 1D-1R single device.

This paper discusses the thermal and signal integrity analysis of two different RRAM architectures. The focus is on the one diode-one resistor (1D1R) single memory cell shown in Fig. 1b, where the word line (WL) and the bit line (BL) are constructed using Nickel bars and bundles of Carbon Nanotubes (CNTs) grown on Nickel substrates. Two architectures are studied: the 4×4×4 1D1R, which serves as the reference case, and the 4×4×4 1D1R-1R1D, which offers a new arrangement for the resistor and the diode as depicted

K. Lahbacha is with the Department of Electrical and Information Engineering, University of Cassino and Southern Lazio, Cassino, Italy (e-mail: khitem.lahbacha@unicas.it).
F. Zayer is with Center for Autonomous Robotic Systems (KUCARS), Khalifa University of Science and Technology (KU), Abu Dhabi, UAE (e-mail: zayer.fakhr@gmail.com).
H. Belgacem, and W. Dghais are with the Laboratory of Electronics and Microelectronics of the University of Monastir, Monastir, Tunisia and with the Higher Institute of Applied Science and Technology of Sousse, University of Sousse, Sousse, Tunisia (e-mail: belgacem.hamdi@gmail.com, waeldghais@ua.pt).
A. Maffucci is with the Department of Electrical and Information Engineering, University of Cassino and Southern Lazio, Cassino, Italy, and with INFN-LNF, Frascati, Italy (e-mail: maffucci@unicas.it).

Authorized licensed use limited to: Universita degli Studi di Cassino. Downloaded on April 05,2024 at 21:49:11 UTC from IEEE Xplore. Restrictions apply.

in Fig. 1a. Different biasing schemes are also explored based on the structure layout and the interconnect materials.

The paper is structured as follows. An electrothermal model in 3D is utilized to conduct electrical and thermal analysis. The models of the equivalent electrical and thermal conductivities of the materials being analyzed are presented in Section II. Section III showcases the use of CNT as interconnect wires instead of Ni materials in the two considered architectures, under various bias schemes. The electrical and thermal distributions of both structures are studied, including the voltage drop along the wires, as well as the thermal crosstalk issues in the vertical and horizontal directions of the crossbar memory. Finally, conclusions are drawn in Section IV.

III. Materials and Methods

A. *Operating principle of a single device*

The reference single device structure is composed of a Ni/HfO_2/Pt resistive switching device with a diode (Pt/TiO_2/Ti) used to limit leakage current during the read/write process. The set process leads to a higher temperature than the reset process, but the thermal distribution follows the same trend. In this paper, only the reset process is considered, driven by the electrothermal effect [9],[10]. To create CNT-based electrodes for the investigated RRAM device, we propose using a collection of a bundle of multi-wall carbon nanotubes (MWCNTs) connected in parallel. This approach effectively reduces the high resistance associated with a single CNT. The conductive filament (CF), formed by oxygen vacancy diffusion, plays a crucial role in the electrical and thermal transport of the RRAM device. Its formation and breakdown correspond to a low-resistive switch (LRS) and a high-resistive switch (HRS), respectively, and can have different shapes due to random behavior. A square-shaped CF has been experimentally proven [12],[13]. Furthermore, numerous individual devices utilizing HfO_2 as their base material have been successfully manufactured [14].

B. *Electrothermal Model*

This paper utilizes COMSOL Multiphysics simulation software to investigate the impact of global changes in parameters on the temperature and voltage distributions in memory cells. The finite element analysis of the simulator enables the design of the elementary memory cell and its crossbar structure, which can then be simulated under electrical and thermal excitation and boundary conditions. The effects of the simulation on each device can be examined by defining the size of the individual elements that make up the model. Thus, the WL and BL electrodes are set to Dirichlet boundary condition $T = 300\ K$ which is represent the ideal heat sink.

Several partial differential equations, including the current continuity equation, Ohm's law, the relation between the electric potential and electrical field, Fourier's law of heat transfer, and the heat source equation, have been solved in COMSOL to obtain the necessary behavior of temperature and electric field. The modules for electric current (1) and heat transfer in solids (2) are coupled in the Multiphysics module (3) to define the source of electromagnetic heat.

$$\nabla \cdot \mathrm{J} = 0 \quad ; \quad \mathrm{J} = \sigma(\mathrm{T})\mathrm{E} \quad ; \quad \mathrm{E} = -\nabla \mathrm{V}, \tag{1}$$

$$\rho(\mathrm{T})\ \mathrm{C_P}(\mathrm{T}) \frac{\partial \mathrm{T(t)}}{\partial \mathrm{t}} - \nabla \kappa(\mathrm{T}) \nabla \mathrm{T(t)} = \mathrm{Q_s}, \tag{2}$$

$$\mathrm{Q_s} = \mathrm{J} \cdot \mathrm{E} \tag{3}$$

Where J is the current density, T is the temperature, and $\sigma(T)$, $\kappa(T)$, $\rho(T)$, and $C_P(T)$, are the temperature-dependent electrical conductivity, thermal conductivity, mass density, and specific heat, respectively and $\mathrm{Q_s}$ is the heat source.

Equation (1) requires modeling of the electrical conductivity in both the oxide and conductive filament. The CF is the dopant region in the memory cell that undergoes a change in resistance states through thermochemical reactions. The unipolar switching behavior occurs through defect migration induced by the local electric field and temperature due to Joule heating. The migration occurs from the anodic interface under a positive top electrode (TE) bias to the cathode side, resulting in the formation of the CF (set process). At this point, the device is in an LRS. Joule heating provides the thermal energy necessary to facilitate ion migration, and several metal oxide conductivities are characterized by the degree of non-stoichiometry of the forming filament [15],[16].

To achieve a more accurate filament model for the reset process, it is essential to consider the filament rupture behavior as a thermal effect rather than an electric field effect, given the highly conductive nature of filaments in an LRS. The conductive filament breaks at high temperature, causing the device to return to HRS. In contrast to our previous work, where the electrical conductivity of the filament was described by a linear law, was temperature-dependent, and was validated through experimental results as demonstrated in [11], in this study we introduce the electrical conductivity of the CF by using Equation (4). This formulation has also been successfully validated and compared against the data presented in [17], as detailed in [19].

$$\sigma(\mathrm{T}) = \sigma_1 \left(1 - \frac{1}{1+\left(\exp\left(-B(T-T_{CRIT})\right)\right)}\right) + \sigma_2, \tag{4}$$

This equation explains the transition from high to low resistive states, depending on the local doping of CF. The high and low conductivity values of the CF are $\sigma_1 = 3300\ \Omega^{-1}cm^{-1}$ and $\sigma_2 = 10\ \Omega^{-1}cm^{-1}$ respectively [17]-[19], with a variation coefficient of B=0.153 to ensure switching behavior from the SET to RESET process. The electrical conductivity of the metal oxide HfO_2 is assumed to be thermally activated by the Arrhenius equation [20]:

$$\sigma(\mathrm{T}) = \sigma_2 \exp\left(-\frac{\mathrm{E_{AC}}}{\mathrm{K_B T}}\right) \tag{5}$$

Authorized licensed use limited to: Universita degli Studi di Cassino. Downloaded on April 05,2024 at 21:49:11 UTC from IEEE Xplore. Restrictions apply.

This equation describes the transition from insulating to metallic conduction in HfO_2, which depends on the atomic percent resulting from local doping. The pre-exponential factor, activation energy, Boltzmann's constant, and local temperature are represented by σ_2, $E_{AC} = 0.05$ eV, $K_B T$, and T, respectively. The equation is based on the assumption that the transition depends on the local doping concentration.

The thermal conductivity of the insulating HfO_2 is given by the linear temperature dependence of k_{HfO} according to [17],

$$K_{HfO} = K_{HfO0}(1 + \lambda(T - T_0)) \quad (6)$$

This paragraph discusses the thermal conductivity of the oxide and the CF in RRAM. The thermal conductivity of the oxide at 300 K is denoted as k_{HfO0}, while the linear thermal coefficient is $\lambda = 10\ mK^{-1}$. The thermal conductivity of the metallic CF, which is made of hafnium, is represented as $K_{Hf} = 23Wm^{-1}K^{-1}$[20]. Although k_{th} might vary slightly from metal to metal, its change induced by temperature is considered negligible in the temperature ranges of 300K - 1500K. The Joule heating in RRAM depends mainly on the ratio of electrical and thermal conductivity, which is constant due to the Wiedemann-Franz law in metals [15],[21]. This is responsible for the universal reset characteristics observed in metal oxide RRAM.

IV. RESULTS DISCUSSION

A. Vertical thermal Crosstalk

The study focuses on analyzing the Ni interconnect in a conventional 4×4×4 structure, which serves as a reference case. The steady-state voltage and thermal distributions are presented in Fig. 2, where external bias voltage sources and grounds are applied to the WL and BL wires, respectively, on one side. In this structure, the first and third layers are active and the second and fourth layers are victim, as the Schottky diodes are reverse biased.

The high voltage drops when using Ni metals as interconnects for RRAM cells causes WL wires to be biased with a high voltage of 1.4 V in order to reset all cells connected on the same WL. However, even with the increase in voltage across Ni wires, a significant portion of the voltage is dropped due to the metal's high resistivity. Therefore, the use of CNT as an interconnect replacing Ni for RRAM integration is proposed to improve thermal integrity and signal performance. The simulation results show that CNTs require a bias of only 1.2 V on one WL side, resulting in a more uniform voltage distribution on the lines of the crossbar compared to Ni wires, and a drop of only about 0.02 V, as proven by values mentioned in Table I.

Fig. 2b describes the thermal analysis of the Ni interconnects in the 3D RRAM crossbar. The increase in applied bias leads to an increase in temperature in the active layers, which can affect the state of the victim cells in the vertical direction due to heat generation. This effect is known as thermal crosstalk and can limit the size of the crossbar and lead to reliability issues with resetting the victim cells when the critical temperature value is reached. The values in Table II confirm the existence of thermal crosstalk in the vertical direction, with temperature values in the victim cells higher than the critical value of 550 K.

The use of CNT as an interconnect can reduce the thermal crosstalk issue in the RRAM crossbar structure. The temperature rise in the victim cells decreases by about 100K-200K compared to Ni wires, which is shown in Table II. This reduction is due to the lower Joule heat generation induced by the metal-CNT interface's critical contact effect, which helps to create low resistive contact with CNTs. The thermal response of the CNT-based structure is presented in Fig. 3b. Therefore, CNT nanowires offer an effective solution for the signal and thermal integrity problem.

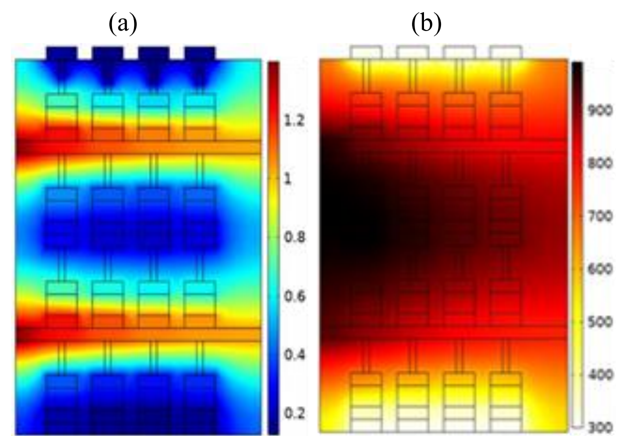

Figure 2. Conventional 4×4×4 array with Ni wires at the steady state : a) electrical potential distribution ; b) temperature distribution.

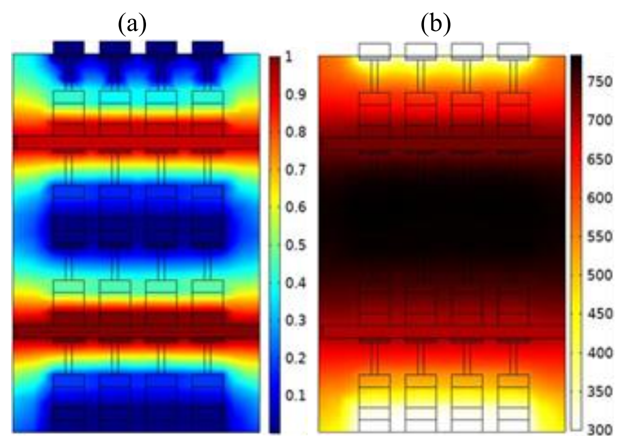

Figure 3. Conventional 4×4×4 array with CNT wires at the steady state : a) electrical potential distribution ; b) temperature distribution.

The authors propose a novel structure [19],[22], and [23], 1D1R-1R1D (shown in Fig. 1a), that rearranges the memory and diode components to address the issue of victim layers. This arrangement places the cells vertically in a complementary pattern, with one diode, one resistor, one resistor, and one diode. As a result, the problem of victim

Authorized licensed use limited to: Universita degli Studi di Cassino. Downloaded on April 05,2024 at 21:49:11 UTC from IEEE Xplore. Restrictions apply.

layers is eliminated. Moreover, the density of the structure increases, as all layers can be switched with the bias of only two WLs. In contrast, the conventional structure requires the biasing of multiple WLs to switch multiple layers. However, to bias all cells connected to the same WL in 1D1R-1R1D, 1.2 V needs to be applied on both sides of the WL due to the voltage drop along the Ni wires (as shown in Fig. 2a). The high resistivity of Ni materials causes this voltage drop, which can disturb cell switching (RESET). Despite this problem, the voltage difference of about 0.7 V across the CFs achieved according to Table I is adequate for the reset operation.

Fig. 3b depicts the steady-state thermal distribution, showing that the two active layers exhibit the highest temperature. Table II provides the CF temperature values of the four layers in the vertical direction. Despite applying the bias on both sides of the WL, the temperature value still exhibits a decrease of approximately 200K compared to the conventional Ni structure, indicating that the thermal response tracks the voltage level. However, the high voltage required to switch the cells results in reduced energy efficiency for the nickel wires. Notably, the maximum temperature in the victim layers shows a significant decrease, with the temperature value of third layer being comparable to the critical value and the temperature value of fourth layer being below the critical value, indicating that the thermal crosstalk issue is resolved.

TABLE I. VOLTAGE LEVELS (V) ACROSS THE CFS ALONG A WL WIRES FOR ALL THE CONSIDERED CASES

Layer #1 Active		Ni	CNT
Conventional Structure	**Bias**	**1.4V**	**1 V**
	Cell1	0.80	0.81
	Cell2	0.79	0.83
	Cell3	0.76	0.83
	Cell4	0.70	0.81
Reverse Structure	**Bias**	**1.2V both sides**	**1V**
	Cell1	0.73	0.74
	Cell2	0.71	0.75
	Cell3	0.71	0.75
	Cell4	0.70	0.74

The proposed structure-based CNT interconnect has a lower applied voltage of approximately 1V on one side of the WL compared to the Ni interconnect. Table I demonstrates that the voltage drop across the CF is minimal (0.01V) and sufficient for resetting all cells, providing an advantage of using CNT in terms of the applied voltage. Additionally, the thermal response depicted in Fig. 4b indicates that the high temperature is localized only in the two active layers with a significant reduction of approximately 100K compared to the Ni wires.

This observation is supported by the results presented in Table II, where the temperature values of the two victim layers are lower than the critical temperature (550K), indicating that the solution based on CNT interconnects mitigates the thermal crosstalk issue in the vertical direction.

TABLE II. MAXIMUM TEMPERATURE (K) OF THE CFS IN VERTICAL DIRECTION FOR ALL THE CONSIDERED CASES.

	Layer state	Ni	CNT
Conventional Structure	**Bias**	**1.4V**	**1 V**
	Layer #1 Active	802.81	639.61
	Layer #2 Victim	972.74	771.22
	Layer #3 Active	960.04	732.52
	Layer #4 Victim	581.00	493.41
Reverse Structure	**Bias**	**1.2V both sides**	**1V**
	Layer #1 Active	675.76	593.82
	Layer #2 Active	757.22	657.39
	Layer #3 Victim	592.01	528.69
	Layer #4 Victim	488.30	440.24

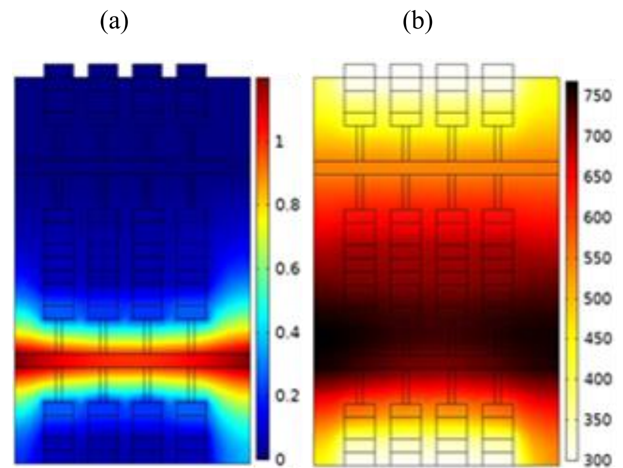

Figure 4. -1R1D 4×4×4 array with Ni wires at the steady state : a) electrical potential distribution ; b) temperature distribution

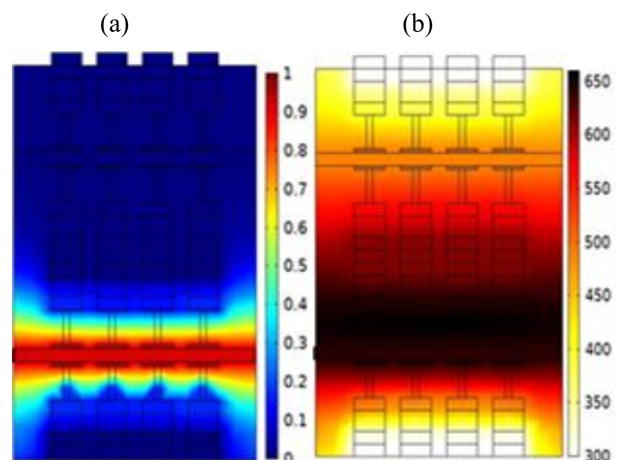

Figure 5. 1D1R-1R1D 4×4×4 array with CNT wires at the steady state: a) electrical potential distribution; b) temperature distribution.

Authorized licensed use limited to: Universita degli Studi di Cassino. Downloaded on April 05,2024 at 21:49:11 UTC from IEEE Xplore. Restrictions apply.

B. Horizontal thermal Crosstalk

The 1D1R-1R1D structure presents a challenge in mitigating thermal crosstalk from a horizontal perspective due to the increased number of active cells connected to the same WL. To address this issue, the structure is polarized vertically from a single WL, while only two WLs are polarized horizontally. This polarization pattern results in the first and third cells being polarized, while the second and fourth cells are unpolarized, as shown in Figs. 6 and 7. The second victim cell is surrounded by four active cells from the two layers. When Ni wires are used, as depicted in Fig. 6a, thermal crosstalk can occur from neighboring cells in the horizontal direction, which can affect the victim cells.

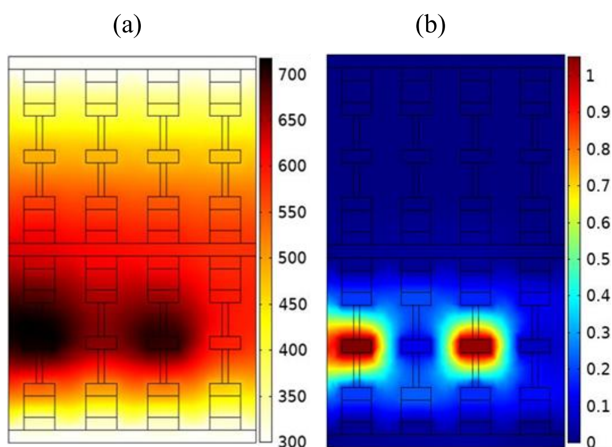

Figure 6. Horizontal Thermal crosstalk of the 4×4×4 1D1R-1R1D array with Ni wires at the steady state : a) temperature distribution ; b) electrical potential distribution.

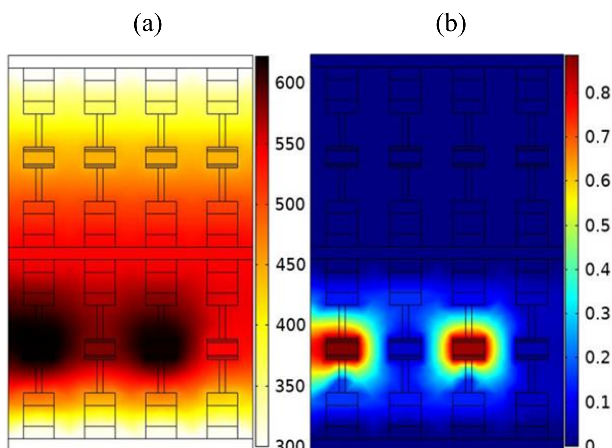

Figure 7. Horizontal Thermal crosstalk of the 4×4×4 1D1R-1R1D array with CNT wires at the steady state : a) temperature distribution ; b) electrical potential distribution.

Based on the thermal behavior observed in Fig. 7 and the temperature values presented in Table III, we can see that the use of CNT interconnects has resulted in a significant reduction in the impact of thermal crosstalk on the victim cells in both horizontal and vertical directions. In particular, for the second victim cell, which is surrounded by four active cells of the two layers, the thermal crosstalk is considerably reduced when CNT is used as the interconnect material, as evidenced by the temperature value of approximately 526.03 K. Similarly, for the fourth victim cell, which is located at the end of the crossbar and affected by neighboring cells on only one side, CNT interconnects have successfully attenuated and resolved the thermal crosstalk problem, with a temperature value of 491.09 K, which is below the critical temperature. In contrast, using Ni wires as interconnects results in a higher temperature rise and a higher risk of thermal integrity issues, as indicated by the temperature values of 539.12 K and 526.03 K for the fourth and second victim cells, respectively. Overall, these results highlight the potential of CNT interconnects for improving the thermal performance and reliability of crossbar-based memory devices.

TABLE III. MAXIMUM TEMPERATURE (K) OF THE CONDUCTING FILAMENTS IN ALL THE CONSIDERED CASES.

Layer #1	2nd victim cell	4th victim cell
Ni	596.79 K	539.12 K
CNT	526.03 K	491.09 K

V. CONCLUSION

The study conducted a thorough investigation of the signal and thermal characteristics of the 3D RRAM crossbar, with a specific focus on the utilization of nickel and carbon nanotubes as interconnect wires for individual devices and monolithic integration. To mitigate voltage drops resulting from the high resistivity of nickel interconnects in the 4×4×4 crossbar array, the study employed bias management techniques, ensuring an adequate voltage level for successful RESET operations in both structures.

In contrast, CNT interconnects exhibited notable improvements in signal and thermal integrity. They demonstrated reduced temperature rise and thermal crosstalk compared to nickel wires, both vertically and horizontally, even at low voltage levels. Additionally, the proposed structure offered advantages such as higher density, eliminating issues associated with reversed biased diodes found in conventional structures, as well as unwanted RESET switching caused by thermal crosstalk between adjacent cells.

ACKNOWLEDGMENT

The authors acknowledge the support by the Project RF Measurements for future communications applications (FutureCom) project (project number 20IND03). This project has received funding from the European Metrology Programme for Innovation and Research (EMPIR programme), co-financed by the Participating States, and from the European Union's Horizon 2020 research and innovation programme.

REFERENCES

[1] Peercy PS. The drive to miniaturization. Nature. 2000 Aug;406(6799):1023-6.

Authorized licensed use limited to: Universita degli Studi di Cassino. Downloaded on April 05,2024 at 21:49:11 UTC from IEEE Xplore. Restrictions apply.

[2] Meijer GI. Who wins the nonvolatile memory race. Science. 2008 Mar 21;319(5870):1625-6.

[3] Govoreanu B, Kar GS, Chen YY, Paraschiv V, Kubicek S, Fantini A, Radu IP, Goux L, Clima S, Degraeve R, Jossart N. 10× 10nm 2 Hf/HfO x crossbar resistive RAM with excellent performance, reliability and low-energy operation. In2011 International Electron Devices Meeting 2011 Dec 5 (pp. 31-6). IEEE.

[4] Park JG, Nam WS, Seo SH, Kim YG, Oh YH, Lee GS, Paik UG. Multilevel nonvolatile small-molecule memory cell embedded with Ni nanocrystals surrounded by a NiO tunneling barrier. Nano letters. 2009 Apr 8;9(4):1713-9.

[5] Sheu SS, Cheng KH, Chang MF, Chiang PC, Lin WP, Lee HY, Chen PS, Chen YS, Wu TY, Chen FT, Su KL. Fast-write resistive RAM (RRAM) for embedded applications. IEEE Design & Test of Computers. 2010 Sep 30;28(1):64-71.

[6] Lee HY, Chen PS, Wu TY, Chen YS, Wang CC, Tzeng PJ, Lin CH, Chen F, Lien CH, Tsai MJ. Low power and high-speed bipolar switching with a thin reactive Ti buffer layer in robust HfO2 based RRAM. In2008 IEEE International Electron Devices Meeting 2008 Dec 15 (pp. 1-4). IEEE.

[7] Lahbacha, K., Zayer, F., Dghais, W., Maffucci, A., & Belgacem, H. (2020, June). Reliable 3D 1D1R-1R1D solution for victim layers in monolithic RRAM integration. In 2020 IEEE International Conference on Design & Test of Integrated Micro & Nano-Systems (DTS) (pp. 1-4). IEEE.

[8] Walczyk C, Walczyk D, Schroeder T, Bertaud T, Sowinska M, Lukosius M, Fraschke M, Wolansky D, Tillack B, Miranda E, Wenger C. Impact of Temperature on the Resistive Switching Behavior of Embedded $\hbox {HfO} _ {2} $-Based RRAM Devices. IEEE transactions on electron devices. 2011 Jul 11;58(9):3124-31.

[9] Zayer, F., Lahbacha, K., Dghais, W., Belgacem, H., de Magistris, M., Maffucci, A., & Melnikov, A. V. (2019, June). Thermal and signal integrity analysis of novel 3D crossbar resistive random-access memories. In 2019 IEEE 23rd Workshop on Signal and Power Integrity (SPI) (pp. 1-4). IEEE.

[10] Zayer, F., Lahbacha, K., Dghais, W., Belgacem, H., de Magistris, M., Melnikov, A. V., & Maffucci, A. (2019, April). Electrothermal analysis of 3D memristive 1D-1RRAM crossbar with carbon nanotube electrodes. In 2019 IEEE International Conference on Design & Test of Integrated Micro & Nano-Systems (DTS) (pp. 1-6). IEEE.

[11] Fakhreddine, Z., Lahbacha, K., Melnikov, A., Belgacem, H., de Magistris, M., Dghais, W., & Maffucci, A. (2020). Signal and Thermal Integrity Analysis of 3-D Stacked Resistive Random-Access Memories. IEEE Transactions on Electron Devices, 68(1), 88-94.

[12] Seok JY, Song SJ, Yoon JH, Yoon KJ, Park TH, Kwon DE, Lim H, Kim GH, Jeong DS, Hwang CS. A review of three-dimensional resistive switching cross-bar array memories from the integration and materials property points of view. Advanced Functional Materials. 2014 Sep;24(34):5316-39.

[13] Larentis S, Nardi F, Balatti S, Gilmer DC, Ielmini D. Resistive switching by voltage-driven ion migration in bipolar RRAM—Part II: Modeling. IEEE Transactions on Electron Devices. 2012 Jun 26;59(9):2468-75.

[14] Saylan, S., Aldosari, H. M., Humood, K., Abi Jaoude, M., Ravaux, F., & Mohammad, B. (2020). Effects of top electrode material in hafnium-oxide-based memristive systems on highly-doped Si. Scientific reports, 10(1), 19541.

[15] Ielmini D. Modeling the universal set/reset characteristics of bipolar RRAM by field-and temperature-driven filament growth. IEEE Transactions on Electron Devices. 2011 Oct 6;58(12):4309-17.

[16] G Jeong DS, Schroeder H, Breuer U, Waser R. Characteristic electroforming behavior in Pt/TiO 2/Pt resistive switching cells depending on atmosphere. Journal of applied physics. 2008 Dec 15;104(12):123716.

[17] Ielmini D, Nardi F, Cagli C. Physical models of size-dependent nanofilament formation and rupture in NiO resistive switching memories. Nanotechnology. 2011 May 16;22(25):254022.

[18] Panzer MA, Shandalov M, Rowlette JA, Oshima Y, Chen YW, McIntyre PC, Goodson KE. Thermal properties of ultrathin hafnium oxide gate dielectric films. IEEE Electron Device Letters. 2009 Oct 30;30(12):1269-71.

[19] Lahbacha, K., Zayer, F., Belgacem, H., Dghais, W., & Maffucci, A. (2021). Performance Enhancement of Large Crossbar Resistive Memories with Complementary and 1D1R-1R1D RRAM Structures. IEEE Open Journal of Nanotechnology, 2, 111-119.

[20] Milošević ND, Maglić KD. Thermophysical properties of solid phase hafnium at high temperatures. International journal of thermophysics. 2006 Mar;27(2):530-53.

[21] Cho E, Han S, Ahn HS, Lee KR, Kim SK, Hwang CS. First-principles study of point defects in rutile Ti O 2− x. Physical Review B. 2006 May 9;73(19):193202.

[22] Lahbacha, K., Belgacem, H., Dghais, W., Zayer, F., & Maffucci, A. (2021, June). Electrothermal RRAM Crossbar Improvement with 3-D CRS and 1D1R-1R1D Architectures. In 2021 IEEE International Conference on Design & Test of Integrated Micro & Nano-Systems (DTS) (pp. 1-5). IEEE.

[23] Lahbacha, K., Belgacem, H., Dghais, W., Zayer, F., & Maffucci, A. (2021, May). High Density RRAM Arrays with Improved Thermal and Signal Integrity. In 2021 IEEE 25th Workshop on Signal and Power Integrity (SPI) (pp. 1-4). IEEE.

Authorized licensed use limited to: Universita degli Studi di Cassino. Downloaded on April 05,2024 at 21:49:11 UTC from IEEE Xplore. Restrictions apply.

View publication stats